Old Dominion University
ODU Digital Commons

Electrical & Computer Engineering Faculty
Publications

Electrical & Computer Engineering

1992

Charge-State Equilibrium and Nonequilibrium Modeling of the Carbon-Pellet Plasma Interaction

A. G. ElCashlan
Old Dominion University

G. A. Gerdin
Old Dominion University

L. L. Vahala
Old Dominion University, lvahala@odu.edu

P. B. Parks

Follow this and additional works at: https://digitalcommons.odu.edu/ece_fac_pubs

Part of the Engineering Commons, and the Plasma and Beam Physics Commons

Charge-state equilibrium and nonequilibrium modeling of the carbon-pellet plasma interaction

A. G. ElCashlan,[a] G. A. Gerdin, and L. L. Vahala
Department of Electrical and Computer Engineering, Old Dominion University, Norfolk, Virginia 23529

P. B. Parks
General Atomics Inc., San Diego, California 92138

Self-consistent equilibrium and nonequilibrium charge-state models are formulated for the spherical expansion of low-Z pellet vapor as an inviscid perfect gas of constant ratio of specific heats being heated volumetrically by the incident electrons of a thermonuclear plasma. The two models are found to be in agreement in the region where the ratio of the ionization length ζ_j to pellet radius r_p is less than unity, but a single parameter, such as the magnitude of this ratio on the sonic surface, is insufficient to determine whether an equilibrium model will be valid for all regions of the ablatant for carbon pellets. Thus a nonequilibrium model is necessary to model the outer regions of the ablatant cloud even for thermonuclear plasma conditions when the cloud is very dense. Also, the effect of the ionization of the ablatant by the incident plasma electrons is found to be 10% or less for even the C^{+3} region in the thermonuclear regime. Finally, although the model used for the healing of the ablatant by the plasma electrons is that for a neutral carbon ablatant, it is shown that the differences in heating by the plasma electrons between this model and that for an ionized ablatant are small.

I. INTRODUCTION

The modeling of the interaction of low-Z pellets with magnetofusion plasmas is important for several reasons. The first is that in the production of the high densities required in tokamaks for achieving long energy confinement times, pellet injection appears to play a key role.[1] Since hydrogen-like refueling pellets cannot penetrate such plasmas as Joint European Torus (JET)[2] without major perturbations, and since low-Z pellets can penetrate similar plasmas such as Tokamak Fusion Test Reactor (TFTR)[3] with apparently no adverse effects, understanding the physics of the interaction of such with magnetofusion plasmas would be important in the design of pellet injectors for more advanced tokamak experiments, such as the proposed high-density Burning Plasma Experiment[4] (BPX) and the International Tokamak Experimental Reactor[5] (ITER). Second, the evaporation cloud can reveal important information about the current distribution in tokamaks since the cloud streams along the magnetic field lines once it is ionized and emits Zeeman-split line radiation.[6,7] Finally, the interaction of the thermonuclear alpha particles and the cloud could yield information about the energy distribution of the alpha particles through the processes of neutralization via double-charge exchange with the vapor,[8] or by the emission of Doppler-shifted radiation when single-electron charge exchange occurs into an excited state of the alpha particle.[9] The shape of the alpha energy distribution is important in determining how well the alpha particles couple their energy to the plasma, and hence the feasibility of ignition. What is being presented

here is an important step in the modeling of the flow of ablatant from these pellets when interacting with thermonuclear plasmas: the inclusion of nonequilibrium charge-state effects.

Previous work. One of the most accepted theories to describe the interaction between hydrogen pellets and magnetic fusion plasmas is the neutral gas shielding (NGS) model.[10] The NGS model is a one-dimensional (1-D) spherically symmetric quasi-steady-state description of the ablating fluid. Hot electrons from the surrounding magneticfusion plasma bombard the pellet surface setting up a neutral gas ablatant cloud on a very short time scale with respect to the motion of the pellet to different plasma conditions. The incident plasma electrons deposit their energy volumetrically through elastic and inelastic collisions with the ablatant cloud. The thickness of the cloud is of a self-regulatory nature, if the cloud gets thicker, the electron heat flux gets attenuated more, so the rate of ablation from the pellet surface decreases, and vice versa. The heating caused by the plasma electrons causes the ablatant to be accelerated from subsonic speeds near the pellet surface to supersonic speeds farther out in the cloud. The model used here basically follows this same procedure.

Thermal dissociation and ionization processes in the ablation cloud act as energy sinks, and consequently slow the ablation rate and modify the cloud profile. A revised version[11] of the NGS model for hydrogen pellets was formulated in which the atomic processes were treated self-consistently by the assumption of local thermodynamic equilibrium (LTE). In this work, this procedure is extended to carbon pellets and both equilibrium and nonequilibrium models for the charge-state populations are considered.

[a] Present address: NASA Langley Research Center, Hampton, Virginia 23665.

A major difference in the ablation mechanism between hydrogen and low-Z material pellets is due to the difference in their sublimation energy. For frozen hydrogen, the sublimation energy is very low so that the plasma electron heat flux must be reduced by the cloud to nearly zero on the pellet surface. Whereas for low-Z pellets, the electron heat flux at the pellet's surface can vary between 25% and 81% of its magnitude when incident on the ablation cloud.[12] Parks et al.[12] have recently developed a model for low-Z pellets based on energy balance. While this model cannot be used to determine spatial profiles of the ablatant charge states, it can be used to establish the properties of the ablatant on the sonic surface. In the present work, this model is used to establish the initial conditions for propagating the fluid equations into the outer regions of the ablation cloud. This procedure will be justified below.

It will be shown below that in the lower-density regions of the cloud that LTE and even equilibrium models, in general, break down. Hence, a major result of this effort has been to incorporate both a collisional-radiational (CR) equilibrium model, and then a CR nonequilibrium model, in order that the results of these calculations could be ultimately compared with experiment and be used to predict the cloud profiles for pellet injection experiments on proposed high-temperature and density magnetic-fusion reactors such as CIT and ITER.

The rest of this paper is organized as follows. In Sec. II, the basic model is outlined, including the treatment of initial conditions, the fluid equations, and the charge-state models, including both the equilibrium and nonequilibrium formulations. In Sec. III, the computational technique is discussed and in Sec. IV a comparison of the results of the equilibrium and nonequilibrium calculations is made for the same set of conditions. In Sec. V, the effect of the direct ionization of the ablatant by the incident plasma electrons is considered (only heating by these electrons and ionization by the ablatant electrons is considered in the basic models[9,11,12]). In Sec. VI, results are discussed and Sec. VII contains the discussion and the conclusions.

II. BASIC MODEL

The structure of the present carbon ablatant model follows closely that of Felber et al.,[11] where the ablatant is treated as an expanding inviscous perfect gas with constant specific heats. In the resulting fluid equations, ionization processes and volumetric ablatant heating by the external plasma electrons are treated self-consistently, where the heating rates are determined by collisional processes, and the gradients in charge-state fractions are determined either from an equilibrium model (as in Felber et al.[11]) or a nonequilibrium model; the appropriateness of each will be discussed in this section. The low-Z pellet model of Parks et al.[12] is used to determine the initial conditions on the sonic surface, which are then used as a starting point for propagating the fluid equations into the outer regions of the ablatant cloud.

In the rest of this section, the initial conditions, the fluid equations, and the charge-state models employed in this work are discussed.

A. Initial conditions

The initial conditions for the steady-state fluid propagation equations are the temperature T_*, density n_*, fraction of the singly ionized charge state f_{1*}, and flow velocity v_*, of the ablatant on the sonic surface and its radius r_* for a given external plasma electron temperature T_e, electron density n_e, and pellet radius r_p. These parameters can be readily obtained from Parks low-Z model,[12] which also contains a self-consistent solution to the Boltzmann equation for the velocity distribution of the external plasma electrons in the cloud.

Vahala et al.[13] tested the assumptions of the low-Z model,[12] by solving the steady flow problem for the interior region between the sonic and the pellet surface by means of a two-parameter shooting code in a manner similar to those used for hydrogen pellets.[10,11] These assumptions were found to be in general agreement with the results of the shooting code calculations, with the exception of the assumption of the existence of LTE on the sonic surface. That is, this assumption was found to break down for the low-density Texas Experimental Tokamak (TEXT)[14] plasma regime and for low-density TFTR experiments (i.e., $n_e < 5 \times 10^{13}$ cm^3).[15] A better agreement with results from these low-Z pellet injection experiments in the low-density regime was reported[13] when zero percentage ionization on the sonic surface or the interior was assumed. Therefore, in the present work, the full low-Z model initial conditions[12] will be assumed for the high-density regime and zero ionization will be assumed on the sonic surface for the low-density regime. It should be noted that injection of the pellets cools the plasma, so the effective values of n_e and T_e "at infinity" in the pellet-ablation problem will probably not correspond to those existing on that flux surface in the plasma before the pellet was injected; the changes in n_e and T_e due to this cooling depend on the specific experimental conditions, and determining these changes in beyond the scope of this work.

B. Fluid equations

To simplify the mass, momentum, and energy conservation equations, the following definitions are made: the average ionic charge as $Z_{av} = \Sigma j f_j$, and the average ionization energy as $Q_{av} = \Sigma Q_j f_j$, where both summations are from $j=1$ to A_z, A_z being the atomic number of the ablatant species, f_j is the fraction of the ablatant in charge state $+j$. Here $Q_j = \Sigma \phi_i$, summed from $i=1$ to j, where ϕ_i is the ionization potential for the ith charge state. Then the steady-state one-dimensional conservation laws for a spherically expanding inviscid perfect gas of constant specific heats can be written as follows:

$$\rho v r^2 = G/4\pi = \text{const}, \tag{1}$$

$$\rho v \frac{dv}{dr} + \frac{dp}{dr} = 0, \tag{2}$$

$$\left(\frac{G}{4\pi r^2}\right)\left(\frac{d}{dr}\right)\left(\frac{\gamma T(1+Z_{av})}{[m(\gamma-1)]} + \frac{v^2}{2} + \frac{Q_{av}}{m}\right) = \frac{dq}{dr}, \tag{3}$$

where m, ρ, v, r, p, and γ are the atomic mass, mass density, fluid velocity, radius, pressure, and the ratio of specific heats of the ablatant, respectively. Here G is the pellet mass ablation rate and q is the plasma electron heat flux. To these equations are coupled the equation of state:

$$p = nT(1 + Z_{av}),\tag{4}$$

and the generalized expression for the gradients in f_j:

$$\frac{df_j}{dr} = R_j(r),\tag{5}$$

where the expression for $R_j(r)$ will vary depending on which model for the charge-state fractions is most appropriate.

Next the variables are normalized to their values on the sonic surface:

$$r' = \frac{r}{r_*}, \quad n' = \frac{n}{n_*}, \quad \theta = \frac{T}{T_*}, \quad p' = \frac{p}{p_*},$$

$$v' = \frac{v}{v_*}, \quad W = v'^2, \quad q' = \frac{q}{q_*}, \quad L = \frac{L_i}{L_*},$$

where $L_i = 1 + Z_{av}$ and v is the velocity of the flow. After some algebra, the governing equations can be expressed as follows:

$$\frac{dW}{dr'} = 2W \frac{[S - 2\theta L/r' - A_* \, dQ_{av}/dr']}{(\theta L - W)},\tag{6}$$

$$\frac{d\theta}{dr'} = \frac{\{S - [(\gamma-1)/2]dW/dr' - A_* dQ_{av}/dr' - (\theta/L_*)dZ_{av}/dr'\}}{L},\tag{7}$$

$$\frac{df_j}{dr'} = \frac{r_* R_j(r')}{(v'v_*)},\tag{8}$$

where $A_* = (\gamma-1)/(\gamma T_* L_*)$ and $S = [q_*/(n_* v_* n' W^{1/2})] \times dq'/dr'$.

The physical significance of the various quantities in Eqs. (6) and (7) can best be seen in Eq. (7), which describes how the energy per unit mass coming from plasma electron heating S, is divided into thermal energy $d\theta/dr'$, flow energy $[(\gamma-1)/2]dW/dr'$, ionization energy $A_* \, dQ_{av}/dr'$, and equipartition of thermal energy due to ionization $(\theta/L)dZ_{av}/dr'$. When this equation is substituted into a solution of the momentum equation [Eq. (2)] for dW/dr', where the equation of state [Eq. (4)] and the conservation of mass [Eq. (1)] have been used, the solution for dW/dr' [Eq. (6)] possesses a singularity as the sonic surface, since the denominator $(\theta L - W)$ involves quantities that are all normalized to one on the sonic surface [see the definitions above Eq. (6)]. This is exactly the same manner as in Ref. 10, which involved no ionization, so the corresponding equations of Ref. 10 [i.e., Eqs. (16) and (17)] are the same as Eqs. (6) and (7), except the terms involving $dQ_{av} \, dr'$ and dZ_{av}/dr' are missing, as would be expected since these terms involve ionization.

C. The plasma-electron heating flux

The plasma-electron heat flux q' at various locations in the cloud is obtained from the appropriate moment of the plasma-electron velocity distribution obtained from a self-consistent solution to the Boltzmann equation for the incident multienergy group plasma electrons (a Maxwellian distribution is assumed here) slowing down (empirical-range model) in the ablatant cloud; this solution is derived in Ref. 12. Hence dq'/dr' and q' are analytically predetermined so q' does not have to be integrated here, as it did in the earlier models for hydrogen pellets.[10,11] While extending the heating model, derived from the empirical-range model valid for neutral atoms, to the outer regions of the ablatant, which are a multiply ionized plasma, is not entirely self-consistent, it will be shown in Appendix A that the differences in the ablatant heating between the empirical-range and plasma models are only logarithmic in nature. The magnitude of these differences is of order 20%–50% for the plasma-pellet conditions considered here; such differences are within the uncertainties in the other cross sections being used in these calculations, so further change does not appear warranted.

D. Charge-state models

The only part of the fluid equations not defined at present is the $R_j(r')$ factor in Eq. (8), which is dependent on the charge-state model. Three types of charge-state models for plasmas are usually considered.[16] LTE at high density, the coronal model at low density, and the collisional-radiative (CR) model in the intermediate region. In the LTE model, it is assumed that collisional processes dominate both ionization and recombination and that the charge state populations depend on the local temperature and density. The criterion for LTE to exist on the electron density for a given charge-state j can be expressed as[17]

$$n_e > 7.8 \times 10^{18}(j+1)^7 [T(eV)/\phi_j]^{1/2} [cm^{-3}].\tag{9}$$

Since this restriction on electron density is so high, it has been found in this study that for significant portions of carbon pellet ablation clouds, this condition is not satisfied. Whereas, the criteria on electron density for the collisional-radiative (CR) model,[16,18]

$$n_e[cm^{-3}] < 10^{16}(T[eV])^{7/2},\tag{10}$$

where τ_j is the ionization time for the jth charge-state species, are found to represent the conditions in the ablatant cloud for the examples considered here. Therefore a CR model has been used here and the following processes have been modeled; collisional ionization, radiative recombination, dielectronic recombination, and three-body recombination. Using this formulation, Eq. (8) can be written as follows.[19]

$$\frac{df_j}{dr'} = \left(\frac{n_* r_*}{v_*}\right) n'_{eL} [f_{j-1} C^{coll}_{j-1} - f_j (C^{coll}_j + \alpha^{tot}_j) + f_{j+1} \alpha^{tot}_{j+1}],\tag{11}$$

where n'_{eL} is the local electron density of the ablatant (i.e., $n'_{eL} = n'Z_{av}$), C_j^{coll} is the collisional ionization rate from charge state j to charge state $j+1$, and α_j^{tot} is the sum of the collisional, radiative, dielectronic recombination rates from charge state j to $j-1$.

The expressions for collisional ionization, collisional recombination, and dielectronic recombination are taken from Post et al.[20] The expression for radiative recombination is taken from Seaton.[21,22] In these expressions, the ionization potentials ϕ_j are reduced by an amount $\Delta\phi = e/(4\pi\epsilon_0\lambda_D)$ due the potential of the ablatant plasma at each location, where λ_D is the local Debye length.[17]

Under charge-state-equilibrium conditions, the sum of the terms in brackets in Eq. (11) is very close to zero, with respect to the magnitude of the individual terms. That is, the effect of the flow rate [the left-hand side of Eq. (11)] is small with respect to the ionization and recombination rates, so the right-hand side of equation is effectively zero. Thus, the local charge state fractions become only a function of the C_j^{coll}'s and the α_j^{tot}'s. That is, for charge-state equilibrium, f_j can be expressed as[23]

$$f_j = \prod_{m=0}^{j-1} \frac{R_{m,m+1}}{\{1 + \Sigma_{l=1}^{Z} \Pi_{m=0}^{l=1} R_{m,m+1}\}}, \quad (12)$$

where

$$R_{m,m+1} = C_m^{coll}/\alpha_{m+1}^{tot}.$$

The dependence of the C_j^{coll}'s and the α_j^{tot}'s on the local ablatant density and temperature,[20-22] now provide the f_j's with their spatial variation implicitly, through the spatial variations of ablatant temperature and density. Thus, for charge-state-equilibrium conditions, the gradients in the f_j's are determined through the spatial variations of density and temperature via the chain rule, as applied to Eq. (12). Whereas for nonequilibrium, Eq. (11) can be used directly.

Applying the chain rule and the conservation relations [i.e., Eqs. (1)–(4) in their normalized form] to Eq. (12), the derivative in the brackets of Eq. (6) may be expressed as

$$\frac{dQ_{av}}{dr'} = U_1 - U_2 \frac{dW}{dr'}, \quad (13)$$

and the last derivative in the brackets of Eq. (7) may be expressed as

$$\frac{dZ_{av}}{dr'} = U_3 - U_4 \frac{dW}{dr'}, \quad (14)$$

where the U_i's are derived in the Appendix A. Inserting these new expressions into Eqs. (6) and (7), the equilibrium versions of these equations are obtained:

$$\frac{dW}{dr'} = \left(\frac{2W}{[\theta L - W(1 + 2A_* U_2)]}\right)\left(S - A_* U_1 - \frac{2\theta L}{r'}\right), \quad (15)$$

and

$$\frac{d\theta}{dr'} = \frac{(S - A_* U_1 - \theta U_3/L_* + \{A_* U_2 + \theta U_4/L_* - [(\gamma-1)/2]\}dW/dr')}{L}. \quad (16)$$

Note that, although the normalized quantities, θ, W, and L approach 1 on the sonic surface, the denominator of Eq. (15), $[\theta L - W(1 + 2A_* U_2)]$, no longer goes to zero there, but instead has a zero inside the sonic surface. This is due to the dependence of dQ_{av}/dr' and dZ_{av}/dr' in the charge-state equilibrium-model on dW/dr' [see Eqs. (13) and (14) and Appendix B]. When these equations are substituted into Eq. (7) and the result is substituted into the solution of the momentum equation [Eq. (2)], where the equation of state [Eq. (5)] and conservation of mass have been used, the denominator of the solution for dW/dr' [Eq. (15)] has the extra term, $-2WA_* U_2$, which pushes the singularity inward. Therefore, initiating these equations on the sonic surface for does not require recourse to l'Hospital's rule, as is the case when this singularity is encountered directly, as in Eq. (6).[10] Indeed, for propagation of these equations outward, as reported here, this singularity is not encountered, and hence poses no problem whatsoever.

As with Eqs. (6) and (7), the physical significance of the various terms in Eqs. (15) and (16) can be identified, using Eqs. (13) and (14) to identify terms involving ion-

ization energy $A_* dQ_{av}/dr'$ [Eq. (13)] and equipartition of thermal energy due to ionization $(\theta/L)dZ_{av}/dr'$ [Eq. (14)]. The other terms have the same significance as before.

E. Criteria for charge-state equilibrium

For a stationary plasma, the criterion for charge-state equilibrium is that the time for an ionization or recombination process to occur must be much smaller than the time it takes the temperature and/or density to change significantly. For a moving plasma, this ionization time for the jth state, τ_j, must be much smaller than the time τ_f that it takes the ablatant to flow to a region of significantly different temperature and/or density. An estimate τ_j can be obtained from[24]

$$\tau_j = 1/(n_{eL} C_{j-1}^{coll}). \quad (17)$$

If the ionization length ζ_j is defined as the local flow velocity times τ_j, then the criterion becomes that ζ_j must be much smaller than a typical flow length, which for this study will be taken to be the pellet radius r_p. The sonic surface ratio ζ_{j*}/r_p ranges from around 10 for typical

TEXT plasmas, to around 1 for typical TFTR plasmas, and to much less than unity for typical BPX plasmas.[13] Hence it appears a nonequilibrium model will be necessary, especially for comparison between the present model and experimental results from TEXT and TFTR. In Sec. IV, results will be presented that confirm this.

III. COMPUTATIONAL TECHNIQUE

Under conditions close to equilibrium, the term in brackets in Eq. (11) is very close to zero, being the difference between large numbers. For the integration of the nonequilibrium equations [i.e., Eqs. (6), (7), and (11)] to be stable, the integration step size must be kept very small, and double precision must be employed. Since most nonequilibrium flow problems involve departure from equilibrium initial conditions, this problem has received much attention.[25–27]

In this study, the fourth-order Runge–Kutta scheme is used. To check the accuracy of the results, the integration step is varied and the resulting solutions are compared. In some cases, the Treanor technique[26] was used to test the accuracy of the results. The integration step used here is $0.001r_*$, and all calculations were performed with double precision on the IBM 3090 mainframe computer at Old Dominion University.

IV. RESULTS: A COMPARISON OF EQUILIBRIUM AND NONEQUILIBRIUM CALCULATIONS

Following the procedures outlined in Sec. III, Eqs. (15) and (16) were integrated for the equilibrium calculation, and Eqs. (6), (7), and (11) were integrated for the nonequilibrium calculations, after having been specifically modified for carbon pellets. For the dq'/dr' factor contained in the definition of S in these equations [see the line just below Eq. (8)], the following expression is derived from the solution to the Boltzmann equation for the carbon ablatant:[12]

$$\frac{dq'}{dr'} = \frac{C_* G(u)}{[W^{1/2}r'^2]}, \quad (18)$$

where C_* is given by

$$C_* = 9.76 \times 10^{-14} M n_* r_* / T_e^{(p+1)}, \quad (19)$$

where M is the atomic mass of the ablatant and $p = 0.72$ (see Ref. 12); this solution is based on the empirical-range formula model for electrons slowing in neutral carbon. The argument u is the normalized thickness of the ablation cloud exterior to the local position in the cloud, and $G(u)$ is given by

$$G(u) = \frac{1}{2} \int_0^\infty \left(\frac{G'(u)[K + \beta(t^{1/\beta} + u)^\beta]}{(t^{1/\beta} + u)} \right) dt, \quad (20)$$

$\beta = 1/(p+1)$ and $K = \beta(p - 1 + \kappa Z)$. Here $t = E/T_e$, where E is the local incident plasma electron energy, and $G'(u)$ is given by
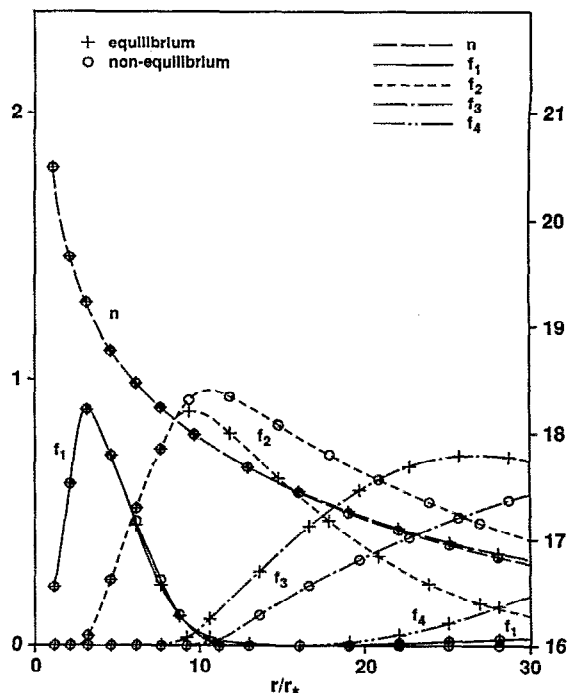

FIG. 1. Comparison of total cloud number density n and charge-state fractions (f_1, f_2, f_3, f_4) for the equilibrium and nonequilibrium models. The pellet radius is 0.05 cm and the background plasma temperature and density are 20 keV and $1.0 \times 10^{14}/\mathrm{cm}^3$, respectively. Here $r_* = 0.067$ cm and $v_* = 5.3 \times 10^5$ cm/sec.

$$G'(u) = t^{(2 + K/\beta)}(t^{1/\beta} + u)^{-K} \exp[-(t^{1/\beta} + u)^\beta]. \quad (21)$$

Finally, Z is the atomic number of the ablatant and κ is given in Ref. 12. As pointed out previously, the extension of this solution, which is strictly only valid for neutral atoms to the outer regions of the ablatant consisting of a multiply ionized plasma, is not entirely self-consistent (see Appendix A). However, as far as the ionization by the plasma electrons is concerned, in the lower-ablatant-density outer regions, there has been little energy loss by the plasma electrons impinging on the ablatant from outside the cloud, so for either model the plasma electron distribution obtained will be essentially a Maxwellian with the temperature of the background plasma.

Some results of these calculations are shown in Fig. 1 for carbon pellets exposed to magnetic-fusion plasma conditions. Equilibrium initial conditions were assumed for both equilibrium and nonequilibrium models, and the equations are switched to those of nonequilibrium at $r = 2r_*$ for these cases. The ionization length on the sonic surface divided by the pellet radius was calculated for each of these cases to quantify them.

In Figs. 1 and 2, the results of both equilibrium and nonequilibrium calculations are shown for comparison for the same external plasma conditions (n_e and T_e) and pellet radius. Note how the change in temperature with radius flattens in regions where there is a rapid increase in f_p as one would expect during a "change of phase," and how these occurrences are more pronounced for the equilibrium
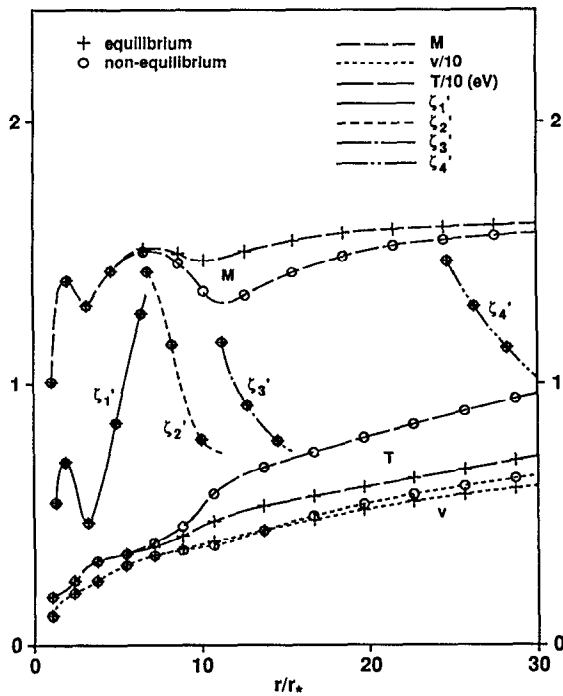
FIG. 2. Normalized ionization ratios, ζ'_i, from the equilibrium model $\{\zeta'_1 = \zeta_1 \times 100, \ \zeta'_2 = \zeta_2, \ \zeta'_3 = \zeta_3/300, \ \zeta'_4 = \zeta_4/2000\}$ and a comparison of Mach number M, flow velocity v, and cloud temperature T for the equilibrium and nonequilibrium models. The background conditions and pellet radius are the same as in Fig. 1.

model, a system with "instantaneous response." The ratio of ζ_{j*}/r_p for this case is 0.004. For hydrogen pellets, this value would be easily sufficient for the equilibrium calculation to be valid everywhere.[28] For the case presented in Fig. 1, there is good agreement between the two calculations in the inner regions ($r < 6r_*$), but breaks down at larger radii. The reason is that as r increases, the density falls, causing an increase in τ_j [see Eq. (17)], and hence ζ_j/r_p. The reason that the same criterion in ζ_{j*}/r_p that held for hydrogen pellets does not hold for all regions of carbon ablation clouds is that hydrogen has only one electron, which is stripped away much closer to the pellet's surface (where equilibrium holds) than for the higher charge states of carbon, so this is really not surprising.

It can be seen, however, that the results from both models for the charge-state fractions f_j are in very close agreement in the region between $2r_*$ and $8r_*$, where one would expect such agreement (at $r = 7r_*$, ζ_2/r_p becomes greater than unity; see Fig. 2). Since there is a considerable difference between the governing equations for the equilibrium and nonequilibrium models, this can be considered as a self-consistency check between the models.

It can also be seen from Fig. 1 by the divergence of the two calculations at $r = 7r_*$ that, even for reactorlike external plasma conditions ($n_e = 10^{14}/\text{cm}^3$ and $T_e = 20$ keV), which result in thicker clouds, higher ablatant densities, and generally smaller τ_j's, the assumption of charge-state equilibrium breaks down in the C^{+2} region, well before the persistent, heliumlike C^{+4} region is reached.

V. IONIZATION BY THE INCIDENT PLASMA ELECTRONS

Up to this point, the plasma electrons responsible for the heating of the ablatant cloud have not been included directly in the ionization process. In regions close to the pellet surface, the density of the ablatant is so high that collisional processes involving the ablatant electrons alone are so much more numerous that they render the effects of the plasma electrons on the ionization process to be negligible. However, in the lower-density exterior regions of the cloud, this is not the case, so these electrons must be included directly.

The ionization rate coefficients for the plasma electrons are treated by integrating numerically an analytical solution to the Boltzmann equation for the plasma electrons f_e obtained from Ref. 12, with the recommended curve fits to the ionization cross sections for electron-impact ionization.[29] In this manner the ionization rate coefficient for the jth charge state by the plasma electrons $C_j^x(f_e)$ is obtained as a function of the radius of the ablatant. Here $C_j^x(f_e)$ is defined as

$$C_j^x(f_e) = n_e S_j^x(f_e)/n_{eL},$$

where

$$S_j^x(f_e) = \langle \sigma v(f_e) \rangle_j.$$

For charge-state-equilibrium conditions, the $R_{m,m+1}$'s in Eq. (12) are now given by

$$R_{m,m+1} = [C_m^{\text{coll}}(T) + C_m^x(f_e)]/\alpha_{m+1}^{\text{tot}}, \qquad (22)$$

where $C_m^{\text{coll}}(T)$ and $\alpha_{m+1}^{\text{tot}}(T)$ are unchanged. This change also modifies the U_j's in equilibrium governing Eqs. (13)–(16); the new U_j's are designated U_j^x, and are given by the same expressions as the U_j's in Appendix B, except that the $R_{m,m+1}$'s are now given by Eq. (22).

For nonequilibrium conditions, the only modification is that the C_j^{coll}'s given in Eq. (11) is now replaced by the expression $[C_j^{\text{coll}}(T) + C_j^x(f_e)]$.

VI. RESULTS

Two comparisons of the results of the nonequilibrium model with and without the ionizing effects of the external plasma electrons are shown in Figs. 3 and 4. In Fig. 3 a comparison is displayed for the same conditions as for Fig. 1 (i.e., $n_e = 10^{14}/\text{cm}^3$, $T_e = 20$ keV, and $r_p = 0.05$ cm). As can be seen in this figure, there is less than a 10% difference, even to the beginning of the C^{+4} for the data shown. This means that, even though the plasma electrons are much more energetic than those of the ablatant, the rate of ionization associated with them is small. However, the densities of the clouds are extraordinarily high, if more modest subthermonuclear conditions exist in the plasma, then the two models diverge, even in the C^{+3} region (see Fig. 4).

VII. DISCUSSION AND CONCLUSIONS

In previous studies,[13] it has been shown that when the ratio of ionization length on the sonic surface ζ_{j*} to pellet

FIG. 3. Comparison of Mach number M, cloud temperature T, and charge-state fractions (f_1, f_2, f_3, f_4) for the nonequilibrium model with and without ionization caused by the plasma electrons. The background conditions and pellet radius are the same as in Fig. 1.
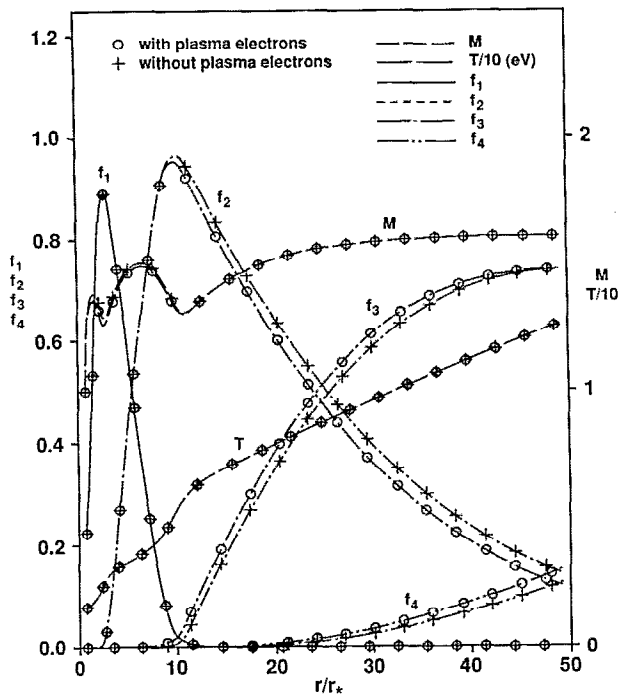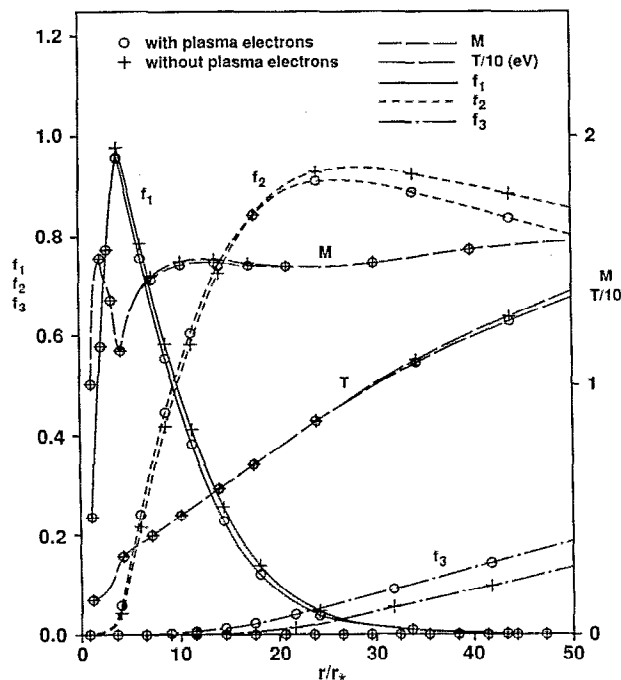

FIG. 4. Comparison of Mach number M, cloud temperature T, and charge-state fractions (f_1, f_2, f_3, f_4) for the nonequilibrium model with and without ionization caused by the plasma electrons. The pellet radius is 0.05 cm and the background plasma temperature and density are 5 keV and $5.0 \times 10^{13}/cm^3$, respectively; $r_* = 0.067$ cm.

radius is small, then equilibrium conditions could be assumed on the sonic surface. The results of the present modeling show that for carbon pellets, while equilibrium conditions persist out to a considerable distance for thermonuclear conditions (to $r = 7r_*$), nonequilibrium effects are important beyond this point, even though the clouds are denser, so that collisional rates are higher, which should minimize equilibrium times and lengths (i.e., $\zeta_{j*}/r_p = 0.004$ for this case); this occurs in the C^{+2} region well before the C^{+4} charge-state region is reached. Since this charge state is considered most important for alpha-particle double-charge-exchange diagnostics because it is heliumlike and therefore should be persistent,[8] it is obvious that nonequilibrium calculations are essential to adequately model the carbon-pellet–plasma interactions to be able to simulate the performance of this diagnostic method.

It is true that this model is only one dimensional and does not take into account the channeling of the ablatant along the magnetic field by magnetic forces; this effect would give higher densities than a pure spherical expansion would predict, hence the predictions for the charge-state distributions, which are dependent on the ablatant density, will be in error in the outer regions of the cloud, where this streaming will occur. Since a spherical expansion model is being used here, one must be careful about predictions for the C^{+4} region which will also be in the outer regions of the ablatant. However, for the present experiments on TFTR, the diameter of the channels of the ablatant flow along the field are typically 5–6 cm,[30,31] which corresponds to 60–120 sonic radii (r_*). Predicting the channel diameter for the thermonuclear case is beyond the scope of this work, but assuming they remain in the $60–120r_*$ range, possibly due to the higher ablatant pressures predicted for thermonuclear conditions, the results shown in the figures may not be so far off. That is, the beginning of the C^{+4} region is reached at $20r_*$ (see Fig. 1), while the ablatant should still be in the spherical expansion phase. Hence the restriction to spherically expanding clouds might not be so severe, even out to the beginning of the C^{+4} region.

A second result of this modeling is that the effects of the external plasma electrons, while playing the most important part in cloud heating, play almost a negligible effect on ionization of the ablatant in the inner regions. This is due to their relatively small number with respect to those of the ablatant, which is especially true for thermonuclear conditions, when the self-regulating mechanism makes the cloud thicker and denser.

ACKNOWLEDGMENT

APPENDIX A: A COMPARISON OF THE ABLATANT HEATING BY THE PLASMA ELECTRONS BETWEEN THE BETHE–BLOCH, THE EMPIRICAL ELECTRON RANGE FORMULA, AND THE PLASMA MODELS

For the two neutral-atom heating models (i.e., the Bethe–Bloch and the empirical electron range models), as

TABLE I. Comparison of electron energy-loss models.

Electron energy [keV]	L_{ER} [eV m²]	L_{BB} [eV m²]	L_{PL} [eV m²]	L_{PL}/L_{ER}
1.0	2.36×10^{-19}	2.66×10^{-19}	3.65×10^{-19}	1.56
3.0	1.07×10^{-19}	1.17×10^{-19}	1.45×10^{-19}	1.35
10.0	4.49×10^{-20}	4.46×10^{-20}	5.10×10^{-19}	1.14
30.0	2.04×10^{-20}	1.77×10^{-20}	1.93×10^{-19}	0.94

TABLE II. A comparison of the Maxwellian averages of electron energy-loss models.

Plasma electron temperature [keV]	I_{ER} [eV² m²]	I_{BB} [eV² m²]	I_{PL} [eV² m²]	I_{PL}/I_{ER}
1.0	2.12×10^{-16}	2.22×10^{-16}	4.10×10^{-16}	1.93
3.0	2.89×10^{-16}	3.08×10^{-16}	4.78×10^{-16}	1.65
5.0	3.33×10^{-16}	3.48×10^{-16}	5.10×10^{-16}	1.53
10.0	4.05×10^{-16}	4.02×10^{-16}	5.52×10^{-16}	1.36
20.0	4.91×10^{-16}	4.56×10^{-16}	5.95×10^{-16}	1.21
30.0	5.50×10^{-16}	4.88×10^{-16}	6.20×10^{-16}	1.13

stated in Ref. 12, the differences in the Bethe–Block[32] and the empirical electron range[33] energy loss formulas, for electrons slowing down in low-Z materials, is less than 10% for electrons, with energy greater than 300 eV. So even though the heating model used here is the empirical-range model, to compare the functional dependence of the neutral atom heating models and that for a plasma, the Bethe–Bloch model will be compared with the plasma model first. The Bethe–Bloch electron energy loss formula may be expressed as[32]

$$\frac{dE}{dx}=\frac{2\pi e^4 Z_a n_a \ln(E/I_a)}{E},\qquad (A1)$$

where Z_a, and n_a are the atomic number and number density of the ablatant species, respectively. I_a is the mean ionization energy for the electrons of the ablatant atom and Bloch found that I_a was approximately $5.5Z_a$.[32]

For plasma electrons slowing down in the ablatant plasma $E > 2T$, where T is the temperature of the ablatant, so the plasma electron energy loss on the ablatant plasma electrons can be expressed as[34]

$$\frac{dE}{dx}=\frac{2\pi e^4 n_{eL}\ln[2\pi(2mE)^{1/2}\lambda_D/h]}{E},\qquad (A2)$$

where m, h, λ_D are the electron mass, Planck's constant, and the local Debye length, respectively. Here n_{eL} is the local ablatant electron density and is equal to $Z_{av}n_a$.

For slowing down on the plasma ions, the ion nuclei play a negligible role,[34] but the bound electrons can not be neglected, so the following model was chosen. Using the idea that the ratio of the ionization potential to the mean ionization potential should be a constant for a given electron configuration, I_z, for a given multiply ionized species of charge state $+Z$, is scaled from I_a, for that neutral-atomic species having the same electron configuration, by the ratio of the ionization potentials, i.e.,

$$I_z=(\phi_z/\phi_a)I_a,\qquad (A3)$$

where

$$A_z-Z=A_a,\qquad (A4)$$

where A_z and A_a are the atomic numbers of the multiply charged ion and the neutral atom with the equivalent electron configuration. Hence, using C^{+2} as an example, $A_z=6$, $Z=2$, so $A_a=4$, or a berylliumlike ionic species, therefore I_2 is taken to be

$$I_2=(\phi_{c+2}/\phi_{Be})I_{Be}=(47.9\text{ eV}/9.32\text{ eV})(5.5\times4).\qquad (A5)$$

Thus the total slowing down in the plasma becomes

$$\frac{dE}{dx}=\frac{2\pi e^4 n_{eL}\ln[2\pi(2mE)^{1/2}\lambda_D/h]}{E}$$
$$+\frac{\Sigma_{z=0}^{A_z}2\pi e^4(A_z-Z)n_z\ln(E/I_z)}{E},\qquad (A6)$$

where the sum in the second term is over the ionic species. Thus, it can be seen from Eqs. (A1) and (A6) that the difference between the plasma and Bethe–Bloch models is basically logarithmic in nature.

To compare these formulas, typical ablatant conditions are taken from Figs. 1–4 to be $n_c\approx10^{17}/\text{cm}^3$, $n_{eL}\approx2.5\times10^{17}/\text{cm}^3$, and $T\approx8$ eV, where n_c is the number density of the ablatant nuclei. The results for the energy loss functions $L_{IJ}(E)=(1/n_c)dE_{IJ}/dx$ for the empirical-range model L_{ER}, the Bethe–Bloch model L_{BB}, and the plasma model L_{PL} are given in Table I for various electron energies.

Since the actual heating is an average over the energy distribution of the incoming plasma electrons, Eqs. (A1), (A6), and the energy-loss function for the empirical range formula where integrated over the electron current per unit energy for a Maxwellian having the external plasma temperature T_e:

$$\frac{dq}{dr}=n_c n_c\frac{1}{4}\int_0^\infty\left(\frac{2E}{m}\right)^{1/2}f_e(E)L_{IJ}(E)dE,\qquad (A7)$$

where $f_e(E)$ is the Maxwellian energy distribution for the plasma electrons, n_e is their number density, and $L_{IJ}(E)$ is the energy-loss formula in question. The results of these integrations have the general form

$$\frac{dq}{dr}=\frac{n_c n_e I_{IJ}}{(2\pi mkT_e)^{1/2}},\qquad (A8)$$

where for the empirical-range model I_{ER} is given by

$$I_{ER}=\Gamma(2-p)2.84\times10^{-18}M[\text{amu}](kT_e[\text{eV}])^{(1-p)},$$
$$[\text{eV m}^2],\qquad (A9)$$

where $p=0.72$,[33] M is atomic mass of the ablatant, and Γ is the gamma function.[35] For the Bethe–Bloch energy-loss formula, I_{BB} is given by

$$I_{BB}=2\pi e^4 Z_a\ln(kT/\kappa I_a),\qquad (A10)$$

where $\kappa = e^c$ and C is Euler's constant. For the plasma model, I_{PL} is given by

$$I_{PL} = 2\pi e^4 \left[\left(\frac{Z_{av} \ln[2\pi(2mkT_e)^{1/2}\lambda_D]}{(h\kappa^{1/2})} \right) \right.$$
$$\left. + \frac{\sum_{z=0}^{A_z}(A_z - Z)n_z \ln(kT_e/\kappa I_z)}{n_c} \right]. \quad (A11)$$

Thus the Maxwellian averaged electron heating for the various models can be compared by evaluating the I_{IJ}'s for various temperatures for the typical ablatant conditions used in obtaining Table I; these are tabulated in Table II.

As can be seen in the Table II, the differences between the heating from the empirical-range model and that for the plasma lie between 20% and 53% for the cases displayed in Figs. 1–4. Since this is well within the uncertainties in the other cross sections used in this research, use of a plasma model would not yield significantly more accurate results.

APPENDIX B: U_j'S GIVEN IN EQS. (13)–(16)

These quantities are useful in the equilibrium solution and represent the derivatives of the f_j's with respect to the local normalized temperature θ and the local ablatant electron density n_{eL}, since these parameters characterize the charge-state equilibrium. Under these conditions, f_j can be expressed as[23]

$$f_j = \frac{\Pi_{m=0}^{j-1} R_{m,m+1}}{(1 + \sum_{l=1}^{z} \Pi_{m=0}^{l-1} R_{m,m+1})}, \quad (B1)$$

where

$$R_{m,m+1} = C_m^{coll}/(\alpha_{m+1}^{coll} + \alpha_{m+1}^{rad} + \alpha_{m+1}^{diel}). \quad (B2)$$

The numerator of Eq. (B2) is the ionization rate for ionization of the mth charge state, and the terms of the denominator of (B2) are the recombination rates for the $(m+1)$th charge state for collisional processes (i.e., three-body recombination), radiative processes, and dielectronic processes, respectively.

All these rates are dependent on the local ablatant temperature, and α_{m+1}^{coll} is dependent on the local ablatant electron density n_{eL}.[20-22] Therefore, the spatial derivative of f_j can be expressed as

$$\frac{df_j}{dr} = \sum_{m=0}^{j-1} \frac{df_j}{dR_{m,m+1}} \left(\frac{dR_{m,m+1}}{d\theta} \frac{d\theta}{dr} \right. $$
$$\left. + \frac{dR_{m,m+1}}{dn_{eL}} \frac{dn_{eL}}{dr} \right). \quad (B3)$$

Here n_{eL} can be expressed in terms of the f_j's as

$$n_{eL} = n \sum_{j=1}^{A_z} jf_j, \quad (B4)$$

thus

$$\frac{dn_{eL}}{dr} = \left(\sum_{j=1}^{A_z} jf_j \right) \frac{dn}{dr} + n \sum_{j=1}^{A_z} j\frac{df_j}{dr}. \quad (B5)$$

Inserting (B5) and (B3)

$$\frac{df_j}{dr} = \left(\sum_{m=0}^{j-1} \frac{df_j}{dR_{m,m+1}} \frac{dR_{m,m+1}}{d\theta} \right) \frac{d\theta}{dr}$$
$$+ \left(\sum_{m=0}^{j-1} \frac{df_j}{dR_{m,m+1}} \frac{dR_{m,m+1}}{dn_{eL}} \right) n \sum_{j=1}^{A_z} jf_j \left(\frac{n^{-1}dn}{dr} \right)$$
$$+ \left(\sum_{m=0}^{j-1} \frac{df_j}{dR_{m,m+1}} \frac{dR_{m,m+1}}{dn_{eL}} \right) n \sum_{j=1}^{A_z} \frac{jf_j}{dr}. \quad (B6)$$

To make this equation more manageable, the following definitions are made:

$$A_j \equiv \left(\sum_{m=0}^{j-1} \frac{df_j}{dR_{m,m+1}} \frac{dR_{m,m+1}}{d\theta} \right), \quad (B7)$$

$$B_j \equiv \left(\sum_{m=0}^{j-1} \frac{df_j}{dR_{m,m+1}} \frac{dR_{m,m+1}}{dn_{eL}} \right) n \sum_{j=1}^{A_z} jf_j, \quad (B8)$$

and

$$C_j \equiv \left(\sum_{m=0}^{j-1} \frac{df_j}{dR_{m,m+1}} \frac{dR_{m,m+1}}{dn_{eL}} \right) n. \quad (B9)$$

Thus, Eq. (B6) can be rewritten as

$$\frac{df_j}{dr} = A_j \frac{d\theta}{dr} + B_j n^{-1} \frac{dn}{dr} + C_j \sum_{j=1}^{A_z} \frac{jdf_j}{dr}. \quad (B10)$$

Next, Eq. (7) is substituted for $d\theta/dr$ in Eq. (B10):

$$\frac{df_j}{dr} = \frac{A_j\{S - [(\gamma-1)/2]dW/dr - A_* dQ_{av}/dr - (\theta/L_*)dZ_{av}/dr\}}{L} + B_j n^{-1} \frac{dn}{dr} + C_j \sum_{j=1}^{A_z} j\frac{df_j}{dr}. \quad (B11)$$

Using the conservation of mass, $nW^{1/2}r^2 = 1$, one finds

$$n^{-1} \frac{dn}{dr} = -\frac{2}{r} - \left(\frac{1}{2W} \right) \frac{dW}{dr}. \quad (B12)$$

Substituting for $n^{-1} dn/dr$ in Eq. (B11), one finds

$$\frac{df_j}{dr} = \frac{A_j\{S - [(\gamma-1)/2]dW/dr - A_* dQ_{av}/dr - (\theta/L_*)dZ_{av}/dr\}}{L} - B_j \left[\frac{2}{r} + \left(\frac{1}{2W} \right) \frac{dW}{dr} \right] + C_j \sum_{j=1}^{A_z} j\frac{df_j}{dr}. \quad (B13)$$

From the definitions of Q_{av} and Z_{av} [see the paragraph before Eq. (1)], one has

$$\frac{dQ_{av}}{dr} = \sum_{j=1}^{A_z} Q_j \frac{df_j}{dr} \tag{B14}$$

and

$$\frac{dZ_{av}}{dr} = \sum_{j=1}^{A_z} j \frac{df_j}{dr}. \tag{B15}$$

Thus Eq. (B13) can be written as

$$\frac{df_j}{dr} = \frac{A_j\{S - [(\gamma-1)/2]dW/dr - A_* dQ_{av}/dr - (\theta/L_*)dZ_{av}/dr\}}{L} - B_j\left[\frac{2}{r} + \left(\frac{1}{2W}\right)\frac{dW}{dr}\right] + C_j\frac{dZ_{av}}{dr}. \tag{B16}$$

To make Eq. (B16) more tractable, the following definitions are employed:

$$D_j = A_j\frac{\{S - [(\gamma-1)/2]dW/dr\}}{L} - B_j\left[\frac{2}{r} + \left(\frac{1}{2W}\right)\frac{dW}{dr}\right], \tag{B17}$$

$$E_j = A_* A_j/L, \tag{B18}$$

and

$$H_j = C_j - (\theta/L_*)A_j/L. \tag{B19}$$

Substituting these definitions into Eq. (B16), one finds

$$\frac{df_j}{dr} = D_j - E_j\frac{dQ_{av}}{dr} + H_j\frac{dZ_{av}}{dr}. \tag{B20}$$

Since a solution for dQ_{av}/dr and dZ_{av}/dr consistent with the equilibrium solution is desired, Eq. (B20) is multiplied first by Q_j and summed over j to obtain one equation, involving dQ_{av}/dr and dZ_{av}/dr:

$$\frac{dQ_{av}}{dr}\left(1 + \sum_{j=1}^{A_z} Q_j E_j\right) - \frac{dZ_{av}}{dr}\left(\sum_{j=1}^{A_z} Q_j H_j\right) = \sum_{j=1}^{A_z} Q_j D_j. \tag{B21}$$

Next, Eq. (B20) is multiplied by j and summed over j to obtain a second equation involving dQ_{av}/dr and dZ_{av}/dr:

$$\frac{dQ_{av}}{dr}\left(\sum_{j=1}^{A_z} j E_j\right) + \frac{dZ_{av}}{dr}\left(1 - \sum_{j=1}^{A_z} j H_j\right) = \sum_{j=1}^{A_z} j D_j. \tag{B22}$$

Equations (B21) and B22) are solved using Kramer's rule, with the results

$$\frac{dQ_{av}}{dr} = \frac{[(\Sigma_{j=1}^{A_z} Q_j H_j)(\Sigma_{j=1}^{A_z} j D_j) + (1 - \Sigma_{j=1}^{A_z} j H_j)(\Sigma_{j=1}^{A_z} Q_j D_j)]}{\Delta}, \tag{B23}$$

$$\frac{dZ_{av}}{dr} = \frac{[(\Sigma_{j=1}^{A_z} j D_j)(1 + \Sigma_{j=1}^{A_z} Q_j E_j) - (\Sigma_{j=1}^{A_z} j E_j)(\Sigma_{j=1}^{A_z} Q_j D_j)]}{\Delta}, \tag{B24}$$

where Δ is the determinant of Eqs. (B20) and (B21), and is given by

$$\Delta = \sum_{j=1}^{A_z} Q_j H_j \sum_{j=1}^{A_z} j E_j + \left(1 + \sum_{j=1}^{A_z} Q_j E_j\right)\left(1 - \sum_{j=1}^{A_z} j H_j\right). \tag{B25}$$

Next, to identify the terms in these solutions involving dW/dr, recall from Eqs. (B17)-(B20), that only the D_j's contain terms proportional to dW/dr. Therefore, the D_j's are redefined to reveal their dependence on dW/dr:

$$D_j \equiv V_j - W_j\frac{dW}{dr}, \tag{B26}$$

where

$$V_j = SA_j/L - 2B_j/r \tag{B27}$$

and

$$W_j = (\gamma-1)A_j/2L + B_j/2W. \tag{B28}$$

Since the solutions for dQ_{av}/dr and dZ_{av}/dr in Eqs. (B23) and (B24) involve $(\Sigma_{j=1}^{A_z} Q_j D_j)$ and $> (\Sigma_{j=1}^{A_z} D_j)$, one multiplies Eq. (A26) first by Q_j and sums over j, to obtain

$$\sum_{j=1}^{A_z} Q_j D_j = \sum_{j=1}^{A_z} Q_j V_j - \frac{dW}{dr}\left(\sum_{j=1}^{A_z} Q_j W_j\right). \tag{B29}$$

Next, one multiplies Eq. (B26) by j and sums over j, with the result

$$\sum_{j=1}^{A_z} j D_j = \sum_{j=1}^{A_z} j V_j - \frac{dW}{dr}\left(\sum_{j=1}^{A_z} j W_j\right). \tag{B30}$$

These expressions are finally substituted into the solutions for dQ_{av}/dr and dZ_{av}/dr in Eqs. (B23) and (B24) to obtain the U_j's:

$$\frac{dQ_{av}}{dr'} = U_1 - U_2 \frac{dW}{dr'} \tag{B31}$$

and

$$\frac{dZ_{av}}{dr'} = U_3 - U_4 \frac{dW}{dr'}, \tag{B32}$$

where the U_i's are given by

$$U_1 = \frac{[\Sigma Q_j H_j \Sigma j V_j + (1 - \Sigma j H_j) \Sigma Q_j V_j]}{\Delta}, \tag{B33}$$

$$U_2 = \frac{[\Sigma Q_j H_j \Sigma j W_j + (1 - \Sigma j H_j) \Sigma Q_j W_j]}{\Delta}, \tag{B34}$$

$$U_3 = \frac{[\Sigma j V_j (1 + \Sigma Q_j E_j) - \Sigma j E_j \Sigma Q_j V_j]}{\Delta}, \tag{B35}$$

$$U_4 = \frac{[\Sigma j W_j (1 + \Sigma Q_j E_j) - \Sigma j E_j \Sigma Q_j W_j]}{\Delta}, \tag{B36}$$

where Δ is given in Eq. (B25), and all the sums are from $j = 1$ to A_z.

[1] M. Greenwald, D. Gwinn, and S. Milora, Phys. Rev. Lett. 53, 353 (1984).

[2] The JET Team, *Plasma Physics and Controlled Nuclear Fusion Research, 1988* (International Atomic Energy Agency, Vienna, 1989), Vol. 1, p. 215.

[3] J. L. Terry, E. S. Marmar, R. B. Howell, J. Snipes, D. K. Owens, G. L. Schmidt, D. K. Mansfield, D. M. Meade, J. D. Strachan, M. G. Bell, M. Bitter, A. Cavallo, P. L. Colestock, P. C. Efthimion, E. D. Fredrickson, R. J. Goldston, B. Grek, R. J. Hawryluk, K. W. Hill, J. C. Hosea, H. Hsuan, A. C. Janos, D. L. Jassby, D. W. Johnson, D. C. McCune, K. M. McGuire, D. Mueller, Y. Nagayama, H. K. Park, A. T. Ramsey, J. Schivell, J. E. Stevens, B. C. Stratton, E. J. Synakowski, G. Taylor, R. Wilson, M. C. Zarnstorff, and M. E. Mauel, *Plasma Physics and Controlled Fusion Research, 1990* (International Atomic Energy Agency, Vienna, 1991), Vol. 1, p. 393.

[4] S. J. Zweben, J. D. Strachan, and K. M. Young, Fusion Technol. 18, 573 (1990).

[5] The ITER Team, *Plasma Physics and Controlled Nuclear Fusion Research, 1988* (International Atomic Energy Agency, Vienna, 1989), Vol. III, p. 233.

[6] E. S. Marmar, J. L. Terry, B. Lipschulz, and J. E. Rice, Rev. Sci. Instrum. 60, 3739 (1989).

[7] J. L. Terry, E. S. Marmar, R. B. Howell, M. Bell, A. Cavallo, E. Fredrickson, A. Ramsay, G. L. Schmidt, B. Stratton, G. Taylor, and M. E. Mauel, Rev. Sci. Instrum. 61, 2908 (1990).

[8] R. K. Fisher, J. S. Leffler, A. M. Howald, and P. B. Parks, Fusion Technol. 13, 536 (1988).

[9] G. Gerdin, Phys. Fluids 30, 3782 (1987).

[10] P. B. Parks and R. J. Turnbull, Phys. Fluids 21, 1735 (1978).

[11] F. S. Felber, P. H. Miller, P. B. Parks, R. Prater, and D. F. Vaslow, Nucl. Fusion 19, 1061 (1979).

[12] P. B Parks, J. S. Leffler, and R. K. Fisher, Nucl. Fusion 28, 477 (1988).

[13] L. L. Vahala, A. G. ElCashlan, G. A. Gerdin, and P. B. Parks, Rev. Sci. Instrum. 61, 3140 (1990).

[14] M. L. Walker, F. C. Anderson, S. C. McCool, K. R. Carter, T. K. Herman, and E. Marmar, Bull. Am. Phys. Soc. 33, 2024 (1988).

[15] E. S. Marmar and J. L. Terry, Rev. Sci. Instrum. 61, 3081 (1990).

[16] R. W. P. McWhirter, in *Plasma Diagnostic Techniques*, edited by R. H. Huddlestone and S. L. Leonard (Academic, New York, 1965), Chap. 5.

[17] H. R. Griem, *Plasma Spectroscopy* (McGraw-Hill, New York, 1964), Chap. 6.

[18] T. F. Stratton, in Ref. 16, Chap. 8.

[19] J. Magill, J. Phys. D 10, 2257 (1977).

[20] D. E. Post, B. V. Jensen, C. B. Tayrt, W. H. Grasberger, W. A. Lokke, Atom. Data Nucl. Data Tables 20, 397 (1977).

[21] M. J. Seaton, Mon. Not. R. Astron. Soc. 119, 81 (1959).

[22] A. Burgess and M. J. Seaton, Mon. Not. R. Astron. Soc. 120, 121 (1960).

[23] J. J. MacFarlane, G. A. Moses, and R. L. Peterson, Nucl. Fusion 29, 27 (1989).

[24] K. N. C. Bray, in *Nonequilibrium Flows*, edited by P. P. Wegener (Marcel Dekker, New York, 1970), Part II, Chap. 3.

[25] H. Lomax and H. E. Bailey, NASA Technical Document No. NASA TN.D.4109, 1967.

[26] C. E. Treanor, Math. Comput. 20, 39 (1966).

[27] E. S. Oran and J. P. Boris, *Numerical Simulation of Reactive Flow* (Elsevier, New York, 1987).

[28] A. G. ElCashlan, Ph.D. dissertation, Old Dominion University, December, 1990, Chap. 4.

[29] K. L. Bell, H. B. Gilbody, J. G. Hughes, A. E. Kingston, and F. J. Smith, J. Phys. Chem. Ref. Data 12, 891 (1983).

[30] R. K. Fisher (private communication, 1991).

[31] J. L. Terry and J. A. Snipes (private communication, 1991).

[32] N. F. Mott and H. S. W. Massey, *Theory of Atomic Collisions*, 3rd ed. (Oxford U. P., London, 1965).

[33] L. Katz and A. S. Penfold, Rev. Mod. Phys. 24, 28 (1952).

[34] B. A. Trubnikov, *Review of Plasma Physics* (Consultants Bureau, New York, 1965), Vol. I, p. 105.

[35] M. Abramowitz and I. A. Stegun, *Handbook of Mathematical Functions* (Dover, New York, 1965), Chap. 6.